Retinal safety of near-infrared lasers in cataract surgery

Jenny Wang
Christopher Sramek
Yannis M. Paulus
Daniel Lavinsky
Georg Schuele
Dan Anderson
David Dewey
Daniel Palanker

SPIE

Retinal safety of near-infrared lasers in cataract surgery

Jenny Wang,^a Christopher Sramek,^b Yannis M. Paulus,^c Daniel Lavinsky,^c Georg Schuele,^d Dan Anderson,^d David Dewey,^d and Daniel Palanker^{b,c}
^aStanford University, Department of Applied Physics, 452 Lomita Mall, Stanford, California 94305
^bStanford University, Hansen Experimental Physics Laboratory, 452 Lomita Mall, Stanford, California 94305
^cStanford University, Department of Ophthalmology, 452 Lomita Mall, Stanford, California 94305
^dOptiMedica Corporation, 1310 Moffett Park Drive, Sunnyvale, California 94089

Abstract. Femtosecond lasers have added unprecedented precision and reproducibility to cataract surgery. However, retinal safety limits for the near-infrared lasers employed in surgery are not well quantified. We determined retinal injury thresholds for scanning patterns while considering the effects of reduced blood perfusion from rising intraocular pressure and retinal protection from light scattering on bubbles and tissue fragments produced by laser cutting. We measured retinal damage thresholds of a stationary, 1030-nm, continuous-wave laser with 2.6-mm retinal spot size for 10- and 100-s exposures in rabbits to be 1.35 W (1.26 to 1.42) and 0.78 W (0.73 to 0.83), respectively, and 1.08 W (0.96 to 1.11) and 0.36 W (0.33 to 0.41) when retinal perfusion is blocked. These thresholds were input into a computational model of ocular heating to calculate damage threshold temperatures. By requiring the tissue temperature to remain below the damage threshold temperatures determined in stationary beam experiments, one can calculate conservative damage thresholds for cataract surgery patterns. Light scattering on microbubbles and tissue fragments decreased the transmitted power by 88% within a 12 deg angle, adding a significant margin for retinal safety. These results can be used for assessment of the maximum permissible exposure during laser cataract surgery under various assumptions of blood perfusion, treatment duration, and scanning patterns. © 2012 Society of Photo-Optical Instrumentation Engineers (SPIE). [DOI: 10.1117/1.JBO.17.9.095001]

Keywords: computational model; damage threshold; femtosecond laser cataract surgery; perfusion; retinal thermal damage.

Paper 12348 received Jun. 1, 2012; revised manuscript received Aug. 14, 2012; accepted for publication Aug. 15, 2012; published online Sep. 14, 2012.

1 Introduction

Several femtosecond laser systems operating at near-infrared (near-IR) wavelengths have recently been developed and approved for clinical use in cataract surgery.[1–3] These systems perform various steps of the surgery, including cutting a circular opening in the anterior lens capsule (capsulotomy), creating the corneal incisions, and segmenting the opacified lens using tightly focused, high-intensity, near-IR laser pulses to ionize and disrupt tissue. Use of these lasers allows for more precise and reproducible capsulotomies and reduced energy during lens emulsification compared to conventional phacoemulsification procedure. In each laser procedure, hundreds of thousands of pulses are applied to produce dense three-dimensional (3-D) patterns for tissue segmentation. Duration of laser surgery is limited by the pulse repetition rate of the laser, which in turn is limited primarily by average power due to safety considerations. Determining damage thresholds for ocular tissues exposed to the laser radiation is critical for the establishment of proper limitation on cutting speed.

Current femtosecond laser cataract systems use near-IR lasers with wavelengths around 1030 to 1064 nm because linear absorption and scattering is relatively low in water and nonpigmented tissues including the cornea, aqueous humor, lens, and vitreous. Thus, the laser light passes through the anterior segment with little effect until it is focused on the lens. However, the retina and choroid are at risk because the retinal pigment epithelium (RPE) and pigmented choroid contain melanosomes that do have significant linear absorption in the near-IR. Light that passes through the focus can reach the retina and choroid and potentially cause damage via three mechanisms: microbubble formation from vaporization,[4] or mechanical shock-wave damage from confined overheating of melanosomes during a single pulse,[5,6] and cumulative thermal damage from prolonged heating of the RPE and choroid.

Rapid overheating of melanosomes by short individual pulses, which can cause damage via microbubbles (sub-μs) or shock-waves (sub-ns), occurs when the retinal radiant exposure per pulse is on the order of 10 to 100 mJ/cm^2.[7,8] In a typical femtosecond laser system for cataract surgery,[1] the numerical aperture (NA) of the focused beam is about 0.1, corresponding to the minimum retinal spot diameter of 2.6 mm or an area of 0.053 cm^2, which would require pulse energy of 530 μJ. Since typical therapeutic pulse energies do not exceed 10 μJ,[1] which is more than an order of magnitude below the single-pulse damage threshold, confined overheating of melanosomes can be disregarded. As a result, cumulative heating of the retina and choroid is the primary mechanism of inadvertent damage during femtosecond laser-assisted cataract surgery. Retinal damage then depends on the average power, treatment pattern, and treatment duration rather than the energy or beam shape of individual pulses.

Another important variable affecting the thermal damage threshold of the retina is the choroidal and retinal blood perfusion. During laser treatment, the eye is fixed in place to avoid eye movement as the pattern is created. This process is often performed using a suction ring, which may raise intraocular

Address all correspondence to: Jenny Wang, Stanford University, Department of Applied Physics, 452 Lomita Mall-Room 136, Stanford, California 94305. Tel: 650-723-0789; Fax: 650-725-8311; E-mail: jywang2@stanford.edu

pressure. A significant increase in pressure can impede or altogether prevent blood flow in the retina and choroid. Reduced cooling by the flow of blood will lead to increased temperatures during lengthy treatments.

A more detailed understanding of temperature dynamics during long treatments with a scanning beam can be gained by numerically solving the heat conduction equation, as previously done for various photocoagulation treatments.[9] Probability of cellular damage during short exposures can be calculated using the Arrhenius model, which assumes that there is a single critical component with the lowest heat tolerance and describes the damage based on rate equation formalism. This method is used for estimating tissue damage thresholds based on the temperature course.[9] Unfortunately, it is known that this model is inaccurate for durations exceeding 1 s, such as femtosecond laser cataract treatments.[10]

ANSI standard Z136.1-2007 and ISO 15004-2:2007 give guidance for the safe use of lasers, and both are widely regarded as gold standards for defining safe operation of lasers in medical devices such as for ocular laser surgery.[11–13] These standards are based on a collection of published data regarding damage threshold measurements in various animal models. These cover a wide spectrum of wavelengths, as well as a broad range of laser parameters: pulse duration, repetition rate and length of exposure, beam size, and others. However, despite all the literature available, there is still a lack of detailed measurements for near-IR (1030 to 1064 nm) ocular exposures similar to those occurring during femtosecond laser-assisted cataract surgery, where a large beam (> 1 mm) is rapidly scanned over the retina for an extended period of time ($\sim$10 s). As a result, very conservative standards are applied to the procedure and limit cutting speed to below what may be necessary. For example, applying current ANSI standards for a typical cataract surgery system (see Sec. 2.4 later in this paper for further discussion) limits the average laser power to 0.25 W, thereby extending treatment time to longer than 15 s.

In this paper, we experimentally determine the optical threshold power for retinal damage *in vivo* at the approximate exposure time, wavelength, and retinal beam size used in cataract surgery. This data is used in a heat conduction model to compute the threshold temperature course that leads to retinal damage in both normally perfused and nonperfused tissue. We then use the same heat conduction model to calculate the temperature course produced by various scanning beam patterns used in femtosecond laser-assisted cataract surgery and compare this to the damage threshold temperature course. This allows us to predict damage threshold power for any beam pattern used in cataract surgery. We also measure the magnitude of the beam attenuation from plasma absorption and scattering on residual bubbles in tissue to determine what fraction of incident optical power is relevant for retinal damage.[14] By considering all these rather unique factors, a safety threshold can be established for this new surgical laser technique that is more accurate than that of the current ANSI standards, which are based on various scaling assumptions and interpolations.[11–13]

2 Materials and Methods

2.1 *Laser System*

A beam delivery system was built onto a slit lamp with the retinal spot size characteristics and wavelength similar to those used in femtosecond cataract systems. A 10-W,

continuous-wave, 1030-nm laser was used (YFL-P-10-1030; MPB Communications, Montreal, Canada). The fiber output was collimated at a beam diameter of 2.6 mm ($1/e$). A red diode laser was coaligned for guidance during treatment. Overall transmission of the optical system, including the contact lens, was 36%, so the maximum power that could be delivered to the eye was 3.6 W. A custom LabView (National Instruments, Austin, TX) program was written to control exposure duration using an electronic shutter and to adjust output power by controlling the laser driver current. A power meter (10 A; Ophir Optronics, Jerusalem, Israel) was used to measure the laser power reaching the cornea.

2.2 *Establishing Damage Thresholds*

A total of 11 Dutch-belted rabbits (22 eyes) were used in accordance with the Association for Research in Vision and Ophthalmology Resolution on the Use of Animals in Ophthalmic and Vision Research, with approval from the Stanford University Animal Institutional Review Board. The rabbits were anesthetized using ketamine hydrochloride (35 mg/Kg), xylazine (5 mg/Kg), and glycopyrrolate (0.01 mg/Kg). Pupil dilation was achieved by 1 drop each of 1% tropicamide and 2.5% phenylephrine hydrochloride. Topical tetracaine hydrochloride 0.5% was used for local anesthesia. A contact lens (OMRA-WF; Ocular Instruments, Bellevue, WA) was used with hydroxypropyl methylcellulose as a contact gel. In a rabbit eye, this lens (1.5× laser magnification) provides a retinal beam size that is equal to the aerial size.

To block perfusion in certain laser treatments, a trocar was used to insert a 23-G cannula into the vitreous, glue it in place, and attach it to a bottle of balanced salt solution (BSS). During laser treatment, this bottle was raised $\sim$1.2 m above the rabbit so that intraocular pressure was approximately 90 mm Hg, as measured by tono-pen (AVIA; Reichert Technologies, Buffalo, NY). This pressure is slightly higher than rabbit mean arterial pressure of 80 mm Hg,[15] and therefore, perfusion was effectively blocked by preventing blood flow into the eye. This was confirmed by dilated fundus examination with indirect ophthalmoscopy. Immediately after laser treatment, the infusion line was closed and normal intraocular pressure was restored for observation and imaging. The cannula was removed and the trocar insertion point was closed with a suture.

Ophthalmoscopically visible marker lesions were delivered with a 532-nm PASCAL laser (Topcon Medical Laser Systems, Santa Clara, CA) to provide orientation during IR laser delivery and following evaluation. A total of eight test spots at varying power levels and durations were delivered to each eye. Rabbits were examined clinically with a slit lamp directly after exposure and one day later. The appearance of a minimally ophthalmoscopically visible lesion, either acutely or the day after treatment, was the criterion for retinal damage. In addition, OCT imaging (Spectralis; Heidelberg Engineering, Heidelberg, Germany) was also used to assess potential retinal damage (Fig. 1). A total of 32 measurements were done for 10-s exposures and 26 measurements for 100-s exposures in nonperfused rabbits. For perfused rabbits, 38 measurements were performed for 10-s exposures and 25 for 100-s exposures.

2.3 *Thermal Model*

An axially symmetric model of the rabbit eye was constructed in the finite element analysis package COMSOL 4.1 (COMSOL,
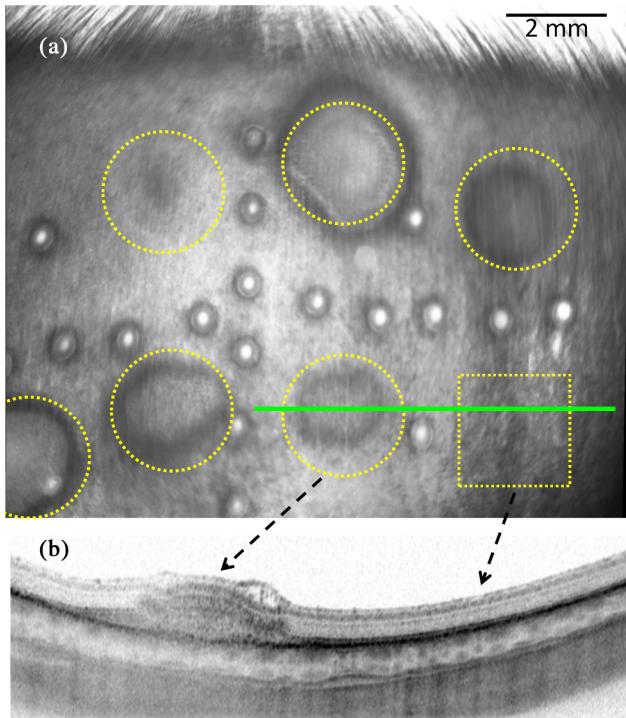
Fig. 1 (a) Red-free scanning ophthalmoscope image of rabbit retina after infrared irradiation of a normally perfused retina. All exposures were for 10 s at the following incident powers (clockwise from top left): 1.26 W, 1.98 W, 1.80 W, 1.98 W, 1.80 W, 1.44 W, and 1.26 W. Clinically visible burns are indicated with the yellow, dotted circles, while invisible exposures are indicated with a square. (b) OCT image of burn one day after treatment. Solid green line indicates OCT position across 1.44 W and 1.26 W exposures.

Burlington, MA). The eye was segmented into 11 layers: cornea, anterior chamber, lens, vitreous, neural retina, RPE, choriocapillaris, pigmented choroid, nonpigmented choroid, sclera, and posterior fat tissue. The basic geometry for the rabbit eye is taken from a chapter by Gwon,[16] while the retinal and choroidal layers are taken from the *in vivo* rabbit model by Sramek et al.[9] The thermal properties of the tissue layers were derived based on the reported water content of each layer,[17–19] assuming that the heat capacity and thermal conductivity would be the scaled average of the properties of water and hydrated proteins[20,21] which make up the remainder of the material. The density of tissue was assumed to be that of pure water or fat[22] at 37°C. The optical absorption coefficients for the retinal and choroidal layers were taken from the 1064 nm data in Hammer et al.[23] Since protein has negligible absorption in the near-IR, the remaining ocular layers were assumed to have absorption coefficients proportional to the water content. The relevant layer thicknesses, thermal properties, and optical properties used in the model are given in Table 1. The radial width of the computational domain was 12 mm.

Temperature dynamics were calculated by numerically solving the bio-heat equation:

$$\rho C_p \frac{\partial T}{\partial t} = \nabla \bullet (k \nabla T) + Q(r, z, t).$$

In the equation, ρ is the density of the tissue, C_p is the heat capacity in the tissue layer, k is the thermal conductivity, and Q is the volumetric heat source term. The initial temperature was 37°C throughout the model and the boundaries of the computation domain had a fixed temperature condition at 37°C. While the cornea is typically cooler than core body temperature, we make this assumption both for simplicity and as a "worst-case scenario" of a very warm treatment environment. The heat source term is a combination of laser heating and cooling from convection of blood in the choroid. Laser heating is treated using the Beer-Lambert law for absorption in a nonscattering medium. As done in a previous model,[24] we can neglect scattering because the width of the beam (1.3 mm radius) is much larger than the axial depth of the pigmented layers that form the primary scattering and absorbing layers (~200 μm). Thus, the heat source term in layer i is given by

Table 1 Computational model parameters based on rabbit eye.

Layer	Thickness (μm)	Water Content	Heat Capacity (J/kg-K)	Thermal Conductivity (W/m-K)	Absorption (cm⁻¹)	Perfusion Rate (s⁻¹)
Cornea	400	75.9	3527	0.51	0.22	0
Anterior chamber	2900	100	4177	0.62	0.22	0
Lens	7600	60	3098	0.43	0.22	0
Vitreous	5900	100	4177	0.62	0.22	0
Neural retina	112	87.8	3848	0.56	0.6	0
Retinal pigment epithelium	4	83.6	3735	0.54	82.4	0
Choriocapillaris	20	83.6	3735	0.54	4.1	2.95–10 s, 6.6–100 s
Pigmented choroid	20	83.6	3735	0.54	82.4	1.18–10 s, 2.64–100 s
Non-pigmented choroid	30	83.6	3735	0.54	4.1	1.18–10 s, 2.64–100 s
Sclera	500	68.8	3336	0.47	0.22	0
Fat	17500	0	2500	0.25	0.063	0

$$Q_i(r, z, t) = \alpha_i \cdot I(r) \cdot e^{-\alpha_i z} - \rho^{\text{blood}} C_p^{\text{blood}} P_i(T - T_o),$$

where α_i is the absorption coefficient of tissue layer i, $I_i(r, z)$ is the Gaussian laser irradiance as a function of radius, ρ^{blood} is the density of blood, C_p^{blood} is the heat capacity, P_i is the perfusion rate in the i'th layer, and T_o is the normal body temperature.

Perfusion is localized to the choriocapillaris and choroid with perfusion rates that are fixed at a 5:2 choriocapillaris to choroid ratio. This is based on the assumption given by Birngruber[25] that all the blood flowing through the choroid must also flow through the smaller volume of choriocapillaris so that the rates of perfusion are inversely proportional to layer thicknesses (Table 1). The absolute perfusion rates were calculated based on the assumption that the damage threshold temperature course for identical exposure durations should be the same, with or without perfusion. The perfusion values were rescaled so that the RMS difference between perfused and nonperfused temperature courses at their respective damage thresholds was minimized. The final values are given in Table 1. This was done separately for 10-s and 100-s exposures because the longer exposure allows more physiological changes to occur, leading to increased blood flow in response to hyperthermia.

2.4 Cataract Surgery Laser Parameters

To model the heat deposited during cataract surgery accurately, we describe here some typical cataract surgery patterns and laser parameters[1] used to guide our calculations. The two patterns are the capsulotomy, a 5-mm cylinder that is 400 μm in depth, and a grid-shaped lens segmentation that is 7 mm in width and 3 mm in depth. Since we are primarily concerned with modeling damage in human eyes, the anatomy of the human eye described by the Gullstrand model[26] is used in determining the irradiance profile. During capsulotomy, the Gaussian laser beam is focused through water or tissue with similar refractive index with an NA of 0.1 (angle for $1/e$) on the anterior lens capsule, which is roughly 20.3 mm above the retina. For the 1030 nm wavelength, this results in a beam radius of ~1.5 mm on the retina. During the lens segmentation, the focus is as low as 17.3 mm above the retina, which produces the minimum beam radius of 1.3 mm. The submerged human eye is assumed to have approximately 19 diopters of refractive power. Based on ray-tracing, a 5-mm circle in the lens produces a ~3.2-mm circle on the retina. The lateral spot spacing is 5 μm during the capsulotomy and 10 μm during the lens segmentation, with an average pulse energy of 6 μJ.[1,2] The axial spot spacing is 10 μm during the capsulotomy and 20 μm during the lens segmentation. To estimate the repetition rate for scanning beam modeling, we first calculate a conservative safety threshold power by assuming a stationary beam and applying the ANSI standard following the retinal irradiance interpretation done by Delori et al.[12,13] For the 1030 nm wavelength and retinal beam radius of 1.3 mm, the maximum permissible power $P = 0.495t^{-0.25}$ W. From the typical pulse energy, pattern size, and spot spacing listed above, we calculate that the total energy $E = 4.17$ J is needed to form both capsulotomy and lens segmentation patterns. Assuming that the whole treatment is carried out with the same pulse energy and repetition rate, the fastest laser procedure that is within the ANSI safety limits can be delivered in $t = E/P = (E/0.495)^{4/3}$. For the total energy E listed above $t = 17$ s. The maximum average power $P = E/t$ is then ~0.25 W and for the pulse energy of 6 μJ, the maximum repetition rate is approximately 42 kHz.

2.5 Scanning Beam Pattern Modeling

The damage thresholds for capsulotomy and lens segmentation patterns are determined based on our previously described thermal model and the reference temperature course calculated for a stationary beam. We make conservative estimates for the damage threshold with the capsulotomy pattern or lens segmentation pattern by requiring that the temperature course remains below the reference damage threshold temperature course during the exposure. Before applying the thermal model, we make several approximations to reduce the complexity of the pulsed, scanning laser pattern.

First, we approximate the gridlike lens segmentation pattern as a series of seven concentric circles to maintain our axisymmetric model. Second, we ignore the vertical displacement of the focused scanning beam and assume that it remains at a fixed plane above the retina. For the capsulotomy, we can reasonably fix the focus plane at the anterior lens capsule (20.3 mm above the retina) because a $\pm$200-mm vertical shift produces only $\pm$1% beam size variation. For the lens segmentation, we make the cautious approximation that the pattern occurs at the lowest actual focal position inside the lens (17.3 mm above the retina) which produces a minimum retinal beam radius of ~1.3 mm. Third, we approximate the pulsed laser as a CW laser with the same average power. The typical femtosecond laser in cataract surgery operates with repetition rates between 10 and 100 kHz, which translates to 10 to 100 μs between pulses. This speed makes the CW approximation valid for the crucial retinal and choroidal layers because the beam radius (~1.3 mm) is large compared to the spot spacing (5 to 10 μm) and the thermal diffusion length for the time between pulses (~2–7 μm).[27]

Finally, we assume that the scanning laser is moving quickly enough that the time-dependent pattern can be approximated by a constant average beam shape. The validity of this approximation depends upon the beam size and how quickly the laser moves around the pattern. For the 5 mm capsulotomy, we can estimate the discrepancy by calculating the temperature rise in an infinite medium with no perfusion for the rotating beam and the average beam using a Green's function approach to solve the heat conduction equation:

$$\frac{\partial T}{\partial t} = \kappa \nabla^2 T + Q(r, z, t)/\rho C_p,$$

$$\Delta T(\vec{r}, t) = \int_0^t ds \iiint dV' G(\vec{r}, \vec{r}', t, s) \varepsilon(\vec{r}', s),$$

where $G(\vec{r}, \vec{r}', t, s) = [4\pi\kappa(t-s)]^{-3/2} Exp[(\vec{r} - \vec{r}')^2 / 4\kappa(t-s)]$, $\kappa = \frac{k}{\rho C_p}$, and $\varepsilon(\vec{r}', s) = Q/\rho C_p$ is the normalized laser-driven heat source term.

We adopt cylindrical coordinates and choose our observation point to lie on the x-axis. Since the absorbing layers are thin, we make the approximation that the heat source term does not depend on z, so the temperature rise becomes

$$\Delta T(r, \theta = 0, t)$$
$$= \int_0^t ds \int_0^{2\pi} d\theta' \int_0^\infty r' dr' G(r, 0, r', \theta', t, s) \varepsilon(r', \theta', s)$$

$$G = [4\pi\kappa(t-s)]^{-3/2} Exp[(r^2 + r'^2 - 2rr' \cos\theta') / 4\kappa(t-s)]$$

$$\varepsilon_{\text{rot}}(r',\theta',s) = \frac{\alpha P}{\pi w^2 \rho C_p}\text{Exp}\left[-\frac{r_0^2 + r'^2 - 2r_0 r'\cos(\theta' - \omega s)}{w^2}\right]$$

$$\varepsilon_{\text{avg}}(r',s) = \frac{\alpha P}{\pi w^2 \rho C_p}\frac{1}{2\pi}\int_0^{2\pi}\text{Exp}\left[-\frac{r_0^2 + r'^2 - 2r_0 r'\cos(\varphi)}{w^2}\right]d\varphi$$

$$= \frac{\alpha P}{\pi w^2 \rho C_p}\text{Exp}\left[-\frac{r_0^2 + r'^2}{w^2}\right]\text{Bessel}I_0\left(\frac{2r_0 r'}{w^2}\right),$$

where w is the $1/e$ beam radius, r_0 is the circle radius, ω is the angular frequency of the rotating beam, and α is the absorption coefficient.

Using Mathematica 8.0 (Wolfram Research, Champaign, IL), we numerically integrate the temperature rise using pattern parameters for the typical 5 mm capsulotomy with a 42 kHz repetition rate and the minimum retinal spot size: $w = 1.3$ mm, $r_0 = 1.6$ mm, and $\omega = 84$ Hz. The thermal parameters for the medium are those of the RPE and choroid (Table 1). Since we are concerned with the maximum possible deviation between average and rotating beams, we choose $r_0 = 1.6$ mm, where the rotating beam is centered as it passes over the observation point and gives the greatest deviation from the average beam. The resulting temperature course is shown in Fig. 2, normalized so that the average temperature rise at 10 s is 1°C. Since the deviation of the rotating beam from the average pattern never exceeds 0.094°C, or 9.4% of the 10 s average temperature rise, we can still use the average beam approximation to calculate a conservative damage threshold by including an additional rotating beam margin in our calculations. This rotating beam margin is calculated for a specific power and pattern in the numerical model as 9.4% of the maximum nonperfused 10 s temperature rise. We can safely apply the same standard in lens segmentation because the pattern scan speed is higher due to the larger spot spacing: 10 μm versus 5 μm. Similarly, increasing the power will

Fig. 3 Computed beam profiles on the retina for equal total power. The CCC profile shown is for a 2.5-mm radius capsulotomy pattern, while the lens segmentation profile is modeled from seven circles with evenly spaced radii from 0.5 to 3.5 mm.

allow higher repetition rates and faster scan speed, which decreases these temperature oscillations.

The average beam shape in the eye for a 1030-nm rotating Gaussian beam as it is focused with 0.1 NA objective to position z_0 and diffraction-limited $1/e$ beam waist $w_0 = 3.3$ μm, and refracted by the human lens with the power of $D = 19$ diopters from a principal plane position at $z_L = 19$ mm, is given by

$$I_{\text{avg}}(r,z) = \frac{I_0}{2\pi}\int_0^{2\pi}\text{Exp}\left[-\frac{R(z)^2 + r^2 - 2\,rR(z)\cos(\varphi)}{w(z)^2}\right]d\varphi$$

$$= I_0\text{Exp}\left[-\frac{R(z)^2 + r^2}{w(z)^2}\right]\text{Bessel}I_0\left(\frac{2\,R(z)r}{w(z)^2}\right),$$

where $w(z) = w_0\sqrt{1 + ((z - z_0)/z_R)^2}$, $z_R = n_{\text{water}}\pi w_0^2/\lambda$, and $R(z) = R_0(1 - (z - z_L)\cdot D)$.

For the capsulotomy pattern, $R_0 = 2.5$ mm and $z_0 = 20.3$ mm, while the lens segmentation is the average of seven such circles with $R_0 = 0.5, 1, \ldots, 3, 5$ mm weighted by R_0 with $z_0 = 17.3$ mm. For comparison, the average radial beam profiles on the retina are shown in Fig. 3.

2.6 Attenuation by Plasma Absorption and Bubble Scattering

There are two additional factors that affect the optical power reaching the retina, which cannot be modeled with continuous-wave radiation: plasma absorption and bubble scattering. To investigate transmission through plasma and residual bubbles accumulating in tissue during successive scans, we used a Ti:Sapphire (Tsunami, Spectra-Physics, Santa Clara, CA) femtosecond laser operating at 1 kHz with $\lambda = 800$ nm and $\tau = 150$ fs. A half-wave plate and polarizing beam splitter were used for attenuation.

Transmitted light was captured on a power meter (PD-300; Ophir Optronics, Jerusalem, Israel) after focusing the beam (NA ~0.07 in air) through a 5% (w/v) gelatin slab (Fig. 4). The power meter was positioned 19 mm from the
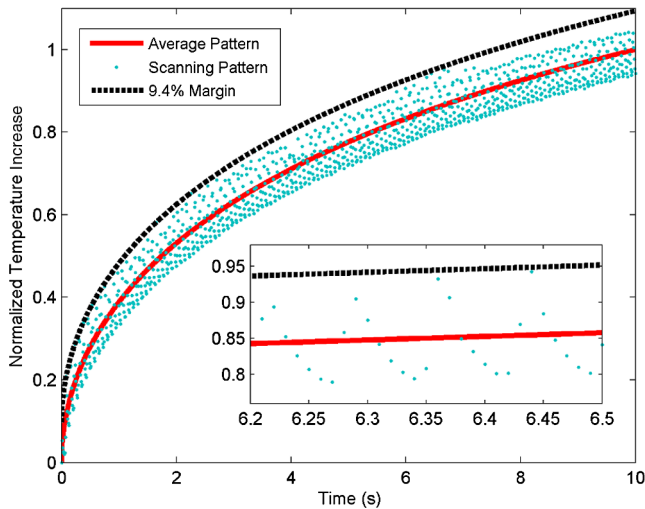

Fig. 2 The normalized temperature increase from the average beam shape for a 5 mm capsulotomy is shown in the solid red line. The normalized temperature increase from the scanning beam shape is shown in blue dots. Both temperature increases are calculated at the observation point $R = 1.6$ mm. The dashed black line shows the maximum fixed margin added to the average beam shape to remain above the scanning shape at all times. This margin is 9.4% of the maximum average temperature rise reached during the 10 s exposure.
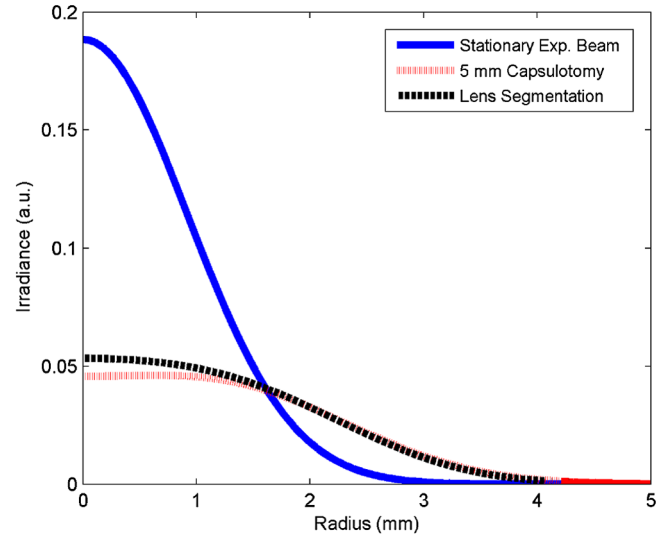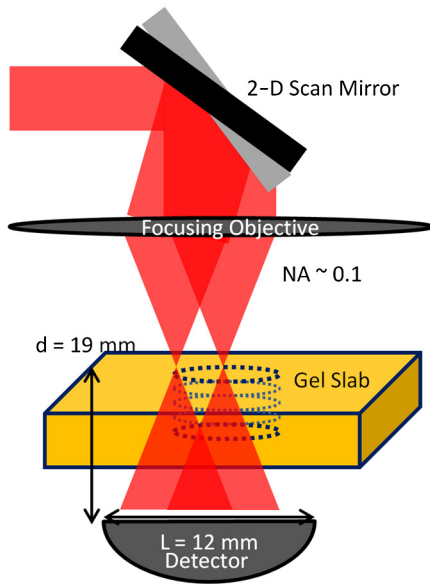
Fig. 4 Experimental setup for measuring transmission through plasma and residual bubbles.

Fig. 5 (a) Plot of laser damage probability after irradiation of normally perfused retina. The probit fits for both exposure durations are shown and 50% damage thresholds of 0.78 W and 1.35 W incident laser power are calculated for 100 s ($n = 25$) and 10 s ($n = 38$), respectively. The gray-shaded area shows the 68% confidence interval (CI) to the fit. (b) Plot of laser damage probability after irradiation of a nonperfused retina. 50% damage thresholds are 0.36 W and 1.04 W for 100 s ($n = 26$) and 10 s ($n = 32$), respectively.

focus of the beam, so that the $12 \times 12 \text{ mm}^2$ active area captures the optical power in an angle of 12 deg from the central ray, twice the size of the focusing angle of the beam. The active area of the power meter is comparable to the computational domain described above. A two-axis scanning mirror (OIM100; Optics In Motion, Long Beach, CA) was used to steer the beam in the desired pattern and a linear translation stage was used to adjust the z-position of the sample.

Residual bubbles trapped in the lens tissue or gelatin are responsible for scattering laser light from subsequent treatment scans. We measured this effect by measuring the average power during successive 4-mm circle scans in the gelatin sample. These scans are axially displaced by 10 μm from one another and were created from bottom to top in the gelatin so that bubble scattering does not inhibit beam focusing and associated plasma formation. The average power was normalized against a scan where gelatin slab was positioned above the laser focus and no plasma breakdown could occur. This no-breakdown power is recorded as the incident power level to account for any intrinsic gel absorption or scattering.

3 Results

3.1 Experimental Damage Thresholds

OCT images of the ophthalmoscopically invisible exposures showed no signs of tissue damage, either acutely or on the day after treatment [Fig. 1(b)], consistent with ophthalmoscopic examination. In contrast, OCT of the ophthalmoscopically visible lesions shows edema or subretinal fluid one day after treatment. These results were also confirmed by histology. The binary results of the retinal damage measurements (yes or no) were fit in MATLAB (MathWorks, Natick, MA) using probit analysis for the four different exposure conditions: perfused 10 s, perfused 100 s, nonperfused 10 s, and nonperfused 100 s. The probability data and fits are shown in Fig. 5. The corneal power at the ED50 threshold for a 10-s exposure with a 1.3-mm $1/e$ radius beam was 1.35 W, with a 68% confidence interval of 1.26 to 1.42 W for perfused treatment and 0.78 W with
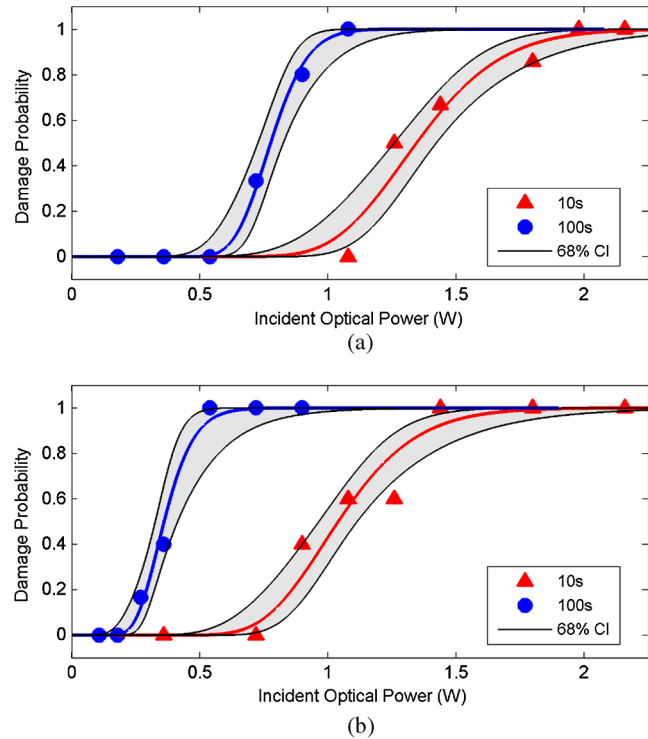
a 68% confidence interval of 0.73 to 0.83 W for nonperfused treatment. For a 100 s exposure, the ED50 powers were 1.04 (0.96 to 1.11) W and 0.36 (0.28 to 0.41) W for perfused and nonperfused treatment, respectively. In our experiment, the highest corneal powers without damage were 1.08 W for 10 s perfused treatment, 0.72 W for 10 s nonperfused treatment, 0.54 W for 100 s perfused treatment, and 0.18 W for 100 s nonperfused treatment.

3.2 ED50 Threshold Temperature Course

The model described in section 2.3 was created in COMSOL 4.1 and a finite element mesh with ~50,000 triangular elements was constructed. To confirm that the mesh was sufficiently fine, the number of elements was doubled and the calculated temperatures showed no significant change. The temperature course was plotted for the hottest point in the eye. The spatial temperature profile (Figs. 6 and 7) shows that the hottest point is at the center of the laser spot in the pigmented choroid. Peak temperature rise at the 10-s ED50 damage threshold is 23.8°C perfused and 24.6°C nonperfused, while peak temperature rise at the 100-s ED50 damage threshold is 11.7°C perfused and 12.6°C nonperfused. The perfusion values chosen to match the ED50 temperature courses during 10-s exposures were found to be $P_{cp} = 2.95 \text{ s}^{-1}$ for choriocapillaris and $P_{ch} = 1.18 \text{ s}^{-1}$ for pigmented choroid. For 100-s exposures, these values increased to and $P_{cp} = 6.6 \text{ s}^{-1}$ and $P_{ch} = 2.64 \text{ s}^{-1}$.
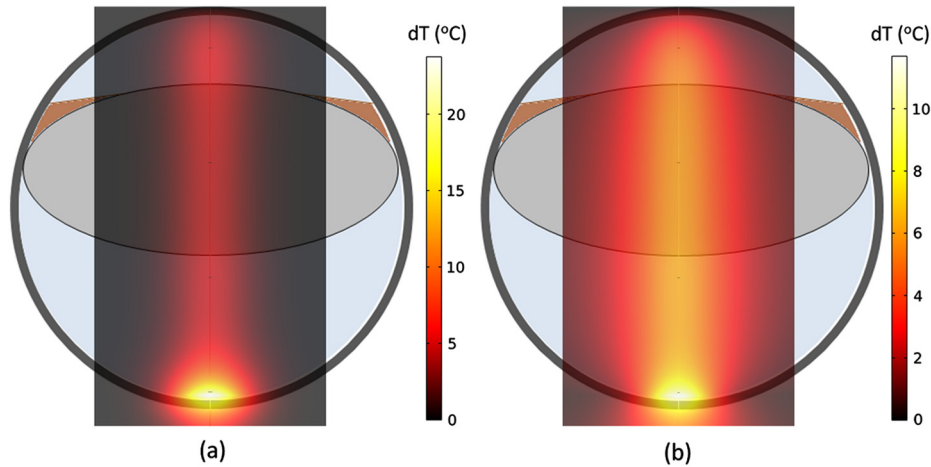
Fig. 6 (a) Map of temperature increase superimposed on a simplified model of the rabbit eye. The temperatures are calculated at the end of 10 s of exposure to a stationary collimated beam at the perfused damage threshold. (b) Temperature rise calculated at the end of 100 s of exposure to a stationary collimated beam at the perfused damage threshold.
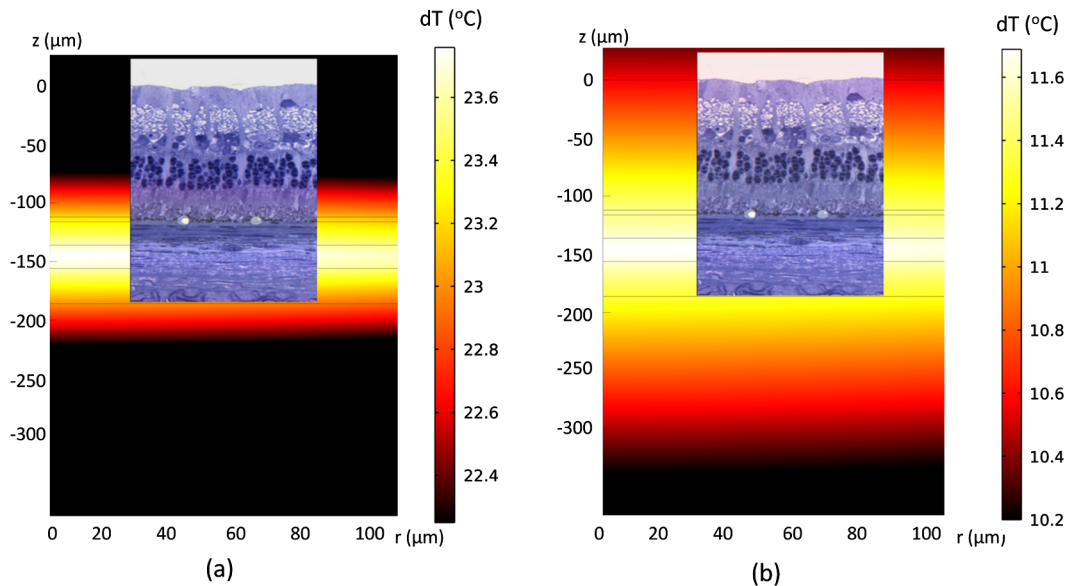

Fig. 7 (a) Map of temperature increase in retinal and choroidal layers. Temperatures are calculated at the end of 10 s of exposure to a stationary collimated beam at the perfused damage threshold with normal rabbit histology of the relevant layers superimposed. (b) Map of temperature increase in retinal and choroidal layers calculated at the end of 100 s of exposure to a stationary collimated beam at the perfused damage threshold.

3.3 Damage Thresholds with Capsulotomy and Lens Segmentation Patterns

Two cataract surgery patterns were modeled as described above. The retinal temperature course was recorded for a range of incident power levels to find the damage threshold power. The quicker capsulotomy pattern was modeled for a 10 s treatment assuming a normally perfused or nonperfused eye. The slower lens segmentation pattern was modeled at both durations (10 and 100 s) under both perfusion conditions. The resulting temperature courses for the lens segmentation patterns are shown in Fig. 8, and the predicted ED50 thresholds of retinal damage for these exposure durations are shown in Table 2. It should be noted that the addition of the rotating beam margin causes the pattern temperature courses to exceed the threshold courses within the initial 5% of the exposure. However, this is disregarded because this initial temperature rise is small compared to the final temperature and short compared to the total treatment duration. This analysis was repeated for the "no damage" power levels based on the experimentally observed zero-damage points from the stationary experiments and is also shown in Table 2.

3.4 Plasma Absorption and Scattering on Residual Bubbles

The normalized transmission through plasma and residual bubbles is plotted with a double exponential fit in Fig. 9 for no-breakdown transmitted energies of 4.9 and 10.2 μJ per pulse. The plasma absorption can be estimated from the transmission values of scan 1 (the first scan with laser focus inside the gel). For both pulse energies, the transmission through plasma is approximately 60%. The additional decline in transmission with subsequent scans is most likely due to residual bubbles that were visible during the experiment. After 10 scans, the fits estimate that the transmission declined to 18% and 12%
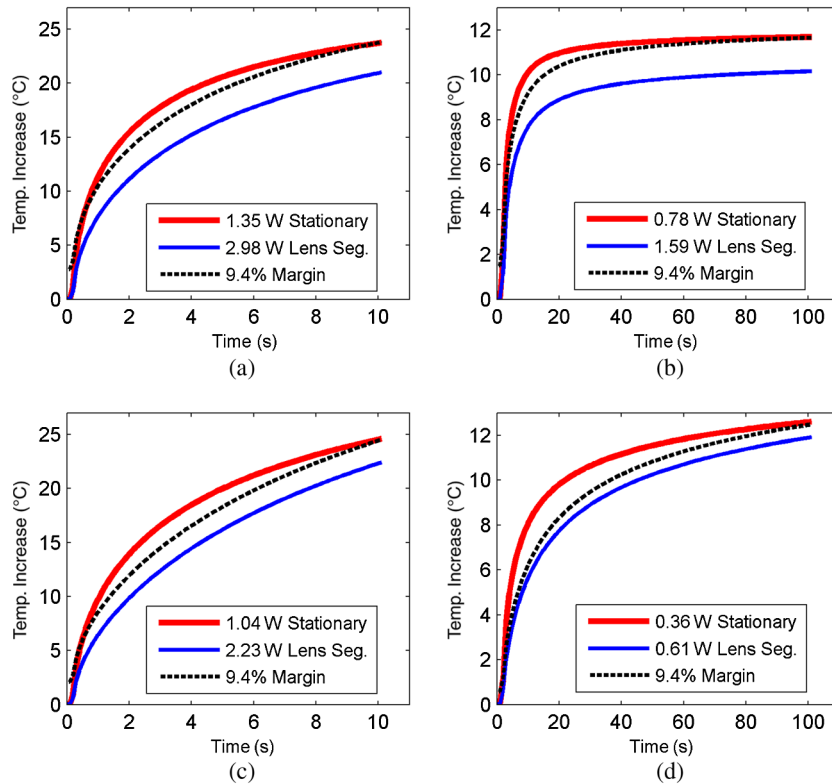
Fig. 8 (a) Temperature course for lens segmentation beam shape and a 10 s exposure in the perfused eye. The 2.98 W lens segmentation threshold (solid blue) indicates the optical power needed to remain below the calculated ED50 perfused tissue damage temperature curve (solid red), with the 9.4% rotating beam error shown with the dotted black line. (b) Temperature course for lens segmentation beam shape and 100 s exposure on the perfused eye showing calculated 1.59 W threshold power. (c) Temperature course for lens segmentation beam shape and a 10 s exposure on the nonperfused eye, showing calculated 2.23 W threshold power. (d) Temperature course for lens segmentation beam shape and 100 s exposure on the nonperfused eye, showing calculated 0.61 W threshold power.

Table 2 Corneal threshold powers for 50% damage probability and zero damage with and without blood perfusion. Stationary beam values are measured while scanning pattern values are estimated based on the computational model.

Pattern (Exposure Time)	ED50 Perfused (W) (68% Confidence Limits)	ED50 Non-Perfused (W) (68% Confidence Limits)	Zero Perfused (W)	Zero Non-Perfused (W)
Stationary (10 s)	**1.35** (1.26–1.42)	**1.04** (0.96–1.11)	1.08	0.72
Stationary (100 s)	**0.78** (0.73–0.83)	**0.36** (0.33–0.41)	0.54	0.18
5 mm capsulotomy (10 s)	3.26	2.44	2.61	1.69
Lens segmentation (10 s)	2.98	2.23	2.37	1.54
Lens segmentation (100 s)	1.59	0.61	1.09	0.30

for 4.9 and 10.2 μJ, respectively. This measurement shows that femtosecond laser cataract surgery has an additional important safety factor that arises from plasma absorption and bubble scattering, which significantly decrease the fraction of laser power reaching the retina under the laser beam.

3.5 Thermal Lensing

In this study, measurements were made for 10 and 100 s exposures, which are useful for predicting the safety of dense, long treatment patterns. Measurements at higher powers and shorter durations would help establish safety limits for higher treatment

speeds. This could not be accomplished in the current study due to the limited power of the laser used. For a 1 s exposure, even the full incident power of 3.6 W was insufficient to produce any visible lesion with the 1.3-mm radius beam. To achieve sufficient intensity for retinal damage, the beam radius was reduced to 300 μm and 110 μm, but the results were inconclusive. Repeating the 10 s measurements at the reduced beam sizes resulted in much higher than expected damage thresholds of 0.54 and 0.36 W and unreasonable calculated temperature rises of ~60°C and ~110°C for the 300 μm and 110 μm beam sizes, respectively.

This irregularity is most probably a result of beam expansion induced by thermal lensing. The radial temperature gradient that
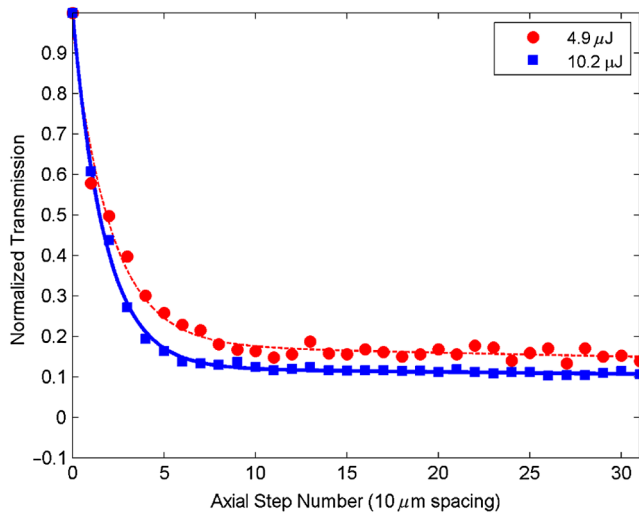
Fig. 9 Plot showing transmitted power after vertically offset circular scans with double exponential fits. The fall in power during the first scan is a result of plasma absorption, while subsequent scans show additional attenuation from residual bubble scattering. The fit function is $a * \exp(-b * x) + c * \exp(-d * x)$.

forms from water absorption of the IR wavelength produces a negative lens due to the negative thermo-optic coefficient of water. This effect has previously been observed with 1150 to 1350-nm laser irradiation.[28,29] While these wavelengths are absorbed more strongly in water than 1030 nm is, the irradiances used in our short exposures are correspondingly higher. The scaling of the effect can be understood from a far-field, thin-lens approximation of thermal lensing for a Gaussian beam.[30] In this approximation, the effective focal length should be proportional to the square of the beam radius and inversely proportional to the laser power. Thus, a negligible effect for large beams can be a strong effect for small beams. To confirm this phenomenon, we imaged the focal zone of the laser beam with ~100 and ~300 μm waist radii through a 17-mm layer of water at low power of 10 mW and at high powers of 400 and 500 mW in steady state. The small beam showed significant expansion of ~1.7 times while the medium beam showed a small expansion of about ~1.1 × with the increase in power, supporting our qualitative picture. Furthermore, since the beam expansion is dynamic, and changes in the beam shape affect the temperature, the system feeds back on itself, and therefore it is nontrivial to calculate the evolution of the beam shape in time. As a result, we were unable to calculate a damage threshold temperature for short (1 s) exposures.

4 Discussion

4.1 Damage Threshold Temperatures

In this study, damage threshold temperatures were calculated indirectly by solving the heat conduction equation. Our threshold maximum temperature rise was 23.8°C for 10 s exposures and 11.7°C for 100 s exposures. Previous thermocouple-based measurements of damage thresholds in the monkey retina[31] indicated the maximum temperature reached for barely visible damage at 10 s in three experiments as 14°C, 15°C, and 21°C.[31] For 100 s exposures, thermocouple-based experiments reported maximum temperatures of 13°C and 8.5°C.[31] The large variability in these measurements reveals the difficulty

in measuring retinal damage threshold temperatures experimentally. Other published long-exposure temperature values can be found based on transpupillary thermotherapy (TTT) parameters. Optoacoustic measurements in rabbit eyes have shown that severe damage occurs with a temperature rise of 21°C at 40 s exposures, while a 10°C rise over 60 s remains below the visible damage threshold.[24] Similarly, computational estimates from human TTT reports suggest that temperature rises of 10°C for 60 s exposures are generally below the damage threshold.[32] Compared to these measurements, our computed values for ED50 are slightly higher than one might expect for 10 s exposures and similar to previous reports of damage for 100 s.

The heat conduction model will provide an accurate measure of temperature rise only if the beam intensity, tissue thermal properties, and optical properties are properly determined. The beam intensity was profiled prior to delivery and is well characterized. There is some uncertainty in the tissue thermal properties: density, heat conductivity, and heat capacity. In this model, we derived them for each tissue layer from reported water content, which made them somewhat different from those in previously reported models.[22,33,34] A careful measurement of these properties is likely to improve temperature calculations slightly, but the greatest source of uncertainty is the absorption coefficients. These are not as easily defined and vary by position in the eye, from subject to subject and from species to species. For more reliable temperature data, recent work on real-time monitoring of retinal temperature in patients[35] could be adopted in cataract surgery systems to establish more accurate damage threshold temperatures and ensure that actual temperatures remain safely below these thresholds.

Nonetheless, the advantage of matching wavelengths in our measurements to those used in actual femtosecond laser-assisted cataract surgery is that the ratio of deposited heat for the stationary and scanned patterns is independent of the absorption coefficients. Thus, while the calculated temperature course might be misscaled due to uncertain optical properties used in both the stationary beam and average scanning beam shape calculations, they will rescale together and the damage threshold predictions in terms of laser power for actual surgical beam patterns will remain valid.

4.2 Self-Focusing Effects

The validity of the model to predicting cataract surgery thresholds depends on the retinal beam shape matching the expected shape from the Gaussian propagation model. The use of high peak-power femtosecond lasers introduces the possibility of self-focusing, which can reduce the retinal beam size and increase the possibility of retinal damage. If we assume that the nonlinear refractive index of ocular tissues is similar to that of water, $n_2 = 2 \times 10^{-16}$ cm^2/W,[36] the critical power for self-focusing for 1030 nm is $P_{crit} = 3.77\lambda^2/8\pi n_0 n_2 = 6$ MW. For the typical pulse energies of 6 μJ, this peak power will be exceeded for any subpicosecond pulses. However, plasma formation and optical breakdown also produces a defocusing effect that can counteract self-focusing.

To determine the outcome of these opposing effects, we imaged a femtosecond laser operating at 1030 nm with a pulse width of 695 fs focused with a NA of 0.1 into water. The beam profile at the approximate retinal plane (19 mm below the focus) was captured at pulse energies ranging from 16 nJ to 8.2 μJ, and the beam size remained consistent with

the expected Gaussian propagation up to the threshold of dielectric breakdown. Above the breakdown threshold of ~780 nJ, strong scattering was observed that attenuated the beam. From this experiment, we conclude that the retinal beam size of ~700 fs pulses at a 1030-nm wavelength can be modeled safely using Gaussian beam propagation although shorter pulses may require further experimental verification.

4.3 Effect of Intraocular Pressure on Damage Threshold

From our data, it is clear that blood perfusion affects the damage threshold power, especially at longer exposures. At 10 s, perfusion increases the damage threshold power by a factor of 1.23, while at 100 s, the damage threshold increases by a factor of 2.2. The technique of temporarily blocking perfusion by elevating intraocular pressure (IOP) is one that mimics the potential side effect of the suction ring attached to the eye for fixation during the treatment.

Our fitted perfusion rates of 2.95 s^{-1} in the choriocapillaris and 1.18 s^{-1} in the choroid for 10 s, and 6.6 s^{-1} and 2.64 s^{-1} for 100 s differ from previously published values of 2.4 s^{-1} in the choriocapillaris and 0.3 s^{-1} in the remaining choroid.[25] However, these values were derived based on thicker choriocapillaris and choroid layers than observed in Dutch-belted rabbit histology.[9] Here, we assume a similarly sized choriocapillaris, 20 versus 25 μm in a previous publication[25] but a much thinner choroid 50 versus 200 μm. If we rescale the literature perfusion rates[25] to account for the different thicknesses, we would obtain 3.0 s^{-1} in the choriocapillaris and 1.2 s^{-1} in the choroid, which is very similar to our 10 s values.

The difference between our calculated 10 and 100 s perfusion rates is a seemingly large factor of 2.6. We suggest that physiological changes may occur due to hyperthermia over the longer time scale that increases blood flow through the choroid. A previous attempt to assess perfusion values for the rabbit eye during a 60 s TTT exposure[37,38] also derived perfusion values that were twice those expected from the previously mentioned experimental measurements in the normal (nonheated) state.[25] Studies on skin heating have shown that convective cooling by blood can increase fivefold based on local sympathetic nerve control of vasodilation.[39] While these changes in the skin occurred on the order of 3 to 5 min, it is possible that such action occurs on a faster time scale in the retina.

4.4 Human Safety Threshold Considerations

It is necessary to consider the differences in thermal damage thresholds in rabbits and humans. Rabbits are widely used to study thermal damage to the retina for therapeutic laser applications, including photocoagulation and TTT. A comparison of the retinal damage thresholds in rabbits and humans allows one to correlate rabbit damage threshold values to those expected in human patients. Retinal photocoagulation thresholds for producing a light burn with a 532 nm, 20 ms laser exposure is about 60 mW (132 μm retinal spot size) in rabbits[40] and 150± 26 mW (100 μm retinal spot size) in human patients.[41] Even disregarding the spot size difference, the light burn threshold in human patients is 2.5 times the corresponding threshold in rabbits. The much higher damage threshold in humans is also seen in long exposures with near-IR irradiation. In rabbits, an 808-nm laser irradiating a 2-mm spot with 120 mW of power over 60 s results in visible retinal damage.[24] In contrast, typical human TTT parameters for lightly pigmented individuals begin at 800 mW for a 3-mm spot and typically do not result in retinal damage during the 60 s exposures.[42] One possible explanation is that most patients undergoing photocoagulation or TTT are older and may have increased scattering through the ocular tissue, which reduces the amount of light at the retina. Yet another possibility is that humans have retinal vasculature and a thicker choroid, which help cool the retina during long exposures. While the explanation for the discrepancy remains elusive, rabbit safety thresholds appear to be a conservative estimate of human safety thresholds.

4.5 Scanning Pattern Damage Thresholds

With the damage thresholds calculated for hypothetical 10 and 100 s scanning patterns, it is useful to compare these values to currently described treatment durations and powers. A 5 mm capsulotomy will require 125,640 spots, while the grid-shaped lens segmentation requires 570,000 spots.[1] Using the typical pulse energy of 6 μJ,[1] we can calculate the total energy for the patterns to be 0.754 and 3.42 J, respectively. From the total energy, we calculate the treatment time for any power limit, and vice versa. For example, the assumed power limit of 0.25 W corresponds to a repetition rate of about 42 kHz and treatment times of 3 and 13.7 s for the capsulotomy and lens segmentation, respectively. Since these patterns are applied consecutively, the total treatment time is 16.7 s. With 0.5 W average treatment power, the repetition rate would double (84 kHz) and the treatment time would decrease to 8.3 s total.

The plot in Fig. 10 compares these power and treatment times with the stationary zero-damage thresholds and the calculated scanning thresholds. From this chart, all of the potential treatment conditions, including the full 0.5 W procedure, have a shorter treatment time and reduced power compared to the
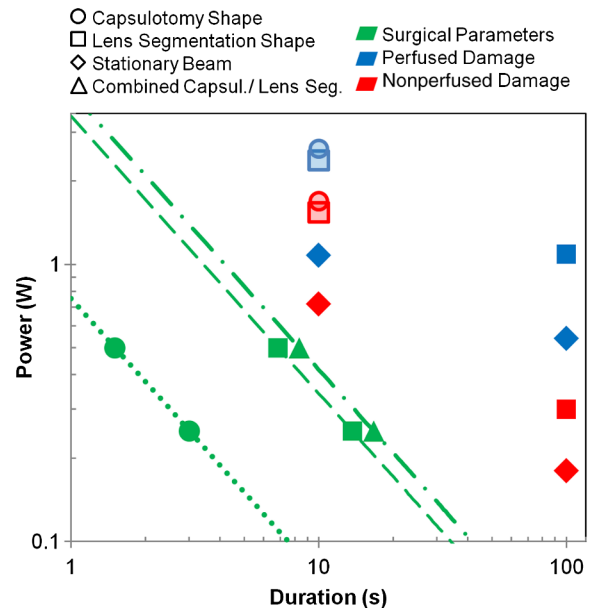

Fig. 10 Log–log chart comparing various treatment parameters with zero damage values. Power and duration values estimated for the total energy needed for real treatment patterns are shown in green. Calculated parameters matching the experimentally observed zero-damage point are shown in blue and red for perfused and nonperfused cases, respectively. The shapes of the data points (circle, square, diamond, and triangle) indicate the pattern being estimated.

appropriate zero-damage threshold, and this holds true even if perfusion is entirely blocked. Additional attenuation factors from plasma absorption and light scattering on residual bubbles can decrease the power reaching the retina by up to 88%. In addition, high intensities in the tightly focused beam in the lens may result in a significant thermal lensing. Such a negative thermal lens would produce a larger retinal spot and further increase the safety.

The logical follow-up, then, is how quickly can the total treatment be delivered while remaining below the damage threshold? To be entirely certain of safety, we stipulate that neither the treatment power nor the treatment duration should exceed those of the predicted damage thresholds. If we cannot be absolutely certain that the beam is scanning properly or that the patient's eye is normally perfused, we must set the safety threshold at 0.72 W, corresponding to the nonperfused stationary zero-damage point (Table 2). This corresponds to a total treatment time of 5.8 s. If the system is scanning normally, we can raise the safety threshold to the nonperfused lens segmentation pattern threshold of 1.54 W, which corresponds to a 2.7 s treatment time. Here, we choose the lens segmentation pattern because it has a lower predicted zero-damage point than the capsulotomy pattern. With normal perfusion, this safety limit jumps to 2.37 W of incident power, giving a further reduced treatment time of 1.76 s. Reduction of treatment time reduces the possibility of errors due to eye movement and helps minimize the patient's discomfort.

5   Conclusions

In this study, we account for a variety of unique factors contributing to the retinal safety of femtosecond laser-assisted cataract surgery. Notably, the effect of perfusion is measured and found to be especially significant for the safety of longer treatment patterns. The design of eye fixation systems, then, is a critical part of retinal safety during laser cataract surgery. Furthermore, plasma absorption and scattering on residual bubbles appear to be very significant additional safety factors that decrease the incident power on the retina several times.

Conventional safety standards of 10% of the ED50 threshold[43] seem excessively cautious since temperature increase scales approximately linearly with absorbed power. A 10% power level results in maximum temperature rises of 2.5°C and 1.2°C for 10 and 100 s, respectively. This is a temperature increase equivalent to a minor fever, and the retina can certainly tolerate much more than this for a treatment lasting 100 s or less. Relying on the most conservative approximations, we make an estimate for the zero-damage threshold for a 10 s patterned treatment to be 1.54 W. A realistic cataract surgery procedure at this power also includes an array of additional safety margins, including blood perfusion, more than fivefold attenuation on plasma and bubbles, and a total duration that is 3.7 times shorter than 10 s. In comparison, relying on the ANSI standard without accounting for scanning would restrict the maximum power to ~0.25 W. From this study, it is clear that higher average powers can be used in femtosecond cataract surgery to improve patient comfort and outcomes with no safety trade-off.

References

1. D. V. Palanker et al., "Femtosecond laser-assisted cataract surgery with integrated optical coherence tomography," *Sci. Translat. Med.* **2**(58), 58ra85 (2010).
2. N. J. Friedman et al., "Femtosecond laser capsulotomy," *J. Cat. Refrac. Surg.* **37**(7), 1189–1198 (2011).
3. Z. Nagy et al., "Initial clinical evaluation of an intraocular femtosecond laser in cataract surgery," *J. Refrac. Surg.* **25**(12), 1053–1060 (2009).
4. R. Brinkmann et al., "Origin of retinal pigment epithelium cell damage by pulsed laser irradiance in the nanosecond to microsecond time regimen," *Lasers Surg. Med.* **27**(5), 451–464 (2000).
5. C. P. Lin and M. W. Kelly, "Cavitation and acoustic emission around laser-heated microparticles," *Appl. Phys. Lett.* **72**(22), 2800–2802 (1998).
6. G. Paltauf, "Photoacoustic cavitation in spherical and cylindrical absorbers," *Appl. Phys. A: Mat. Sci.* **68**(5), 525–531 (1999).
7. C. Framme et al., "Influence of pulse duration and pulse number in selective RPE laser treatment," *Lasers Surg. Med.* **34**(3), 206–215 (2004).
8. C. Cain et al., "Visible lesion threshold dependence on retinal spot size for femtosecond laser pulses," *J. Laser Appl.* **13**(3), 125–131 (2001).
9. C. Sramek et al., "Dynamics of retinal photocoagulation and rupture," *J. Biomed. Opt.* **14**(3), 034007 (2009).
10. D. Simanovskii et al., "Cellular tolerance to pulsed hyperthermia," *Phys. Rev. E* **74**(1), 011915 (2006).
11. ISO, *Ophthalmic Instruments—Fundamental Requirements and Test Methods, Part 2: Light Hazard Protection*, ISO 15004-2:2007, Geneva, Switzerland.
12. ANSI, *American National Standard for Safe Use of Lasers*, ANSI Z136.1-2007, Laser Institute of America, Orlando, FL (2007).
13. F. C. Delori, R. H. Webb, and D. H. Sliney, "Maximum permissible exposures for ocular safety (ANSI 2000), with emphasis on ophthalmic devices," *J. Opt. Soc. Amer. A, Opt. Image Sci. Vis.* **24**(5), 1250–1265 (2007).
14. D. X. Hammer et al., "Shielding properties of laser-induced breakdown in water for pulse durations from 5 ns to 125 fs," *Appl. Opt.* **36**(22), 5630–5640 (1997).
15. J. W. Kiel and W. A. J. van Heuven, "Ocular perfusion pressure and choroidal blood flow in the rabbit," *Invest. Ophthalmol. Vis. Sci.* **36**(3), 579–585 (1995).
16. A. Gwon, "The rabbit in cataract/IOL surgery," in *Animal Models in Eye Research*, P. A. Tsonis, Ed., pp. 184–204, Elsevier, San Diego (2008).
17. V. V. Tuchin et al., "Eye tissues study," *Proc. SPIE* **4427**, 41–46 (2001).
18. R. S. Kadam and U. B. Kompella, "Influence of lipophilicity on drug partitioning into sclera, choroid-retinal pigment epithelium, retina, trabecular meshwork, and optic nerve.," *J. Pharm. Exper. Ther.* **332**(3), 1107–1120 (2010).
19. H. Davson, "The hydration of the cornea," *Biochem. J.* **59**(1), 24–28 (1955).
20. P. H. Yang and J. A. Rupley, "Protein-water interactions. Heat capacity of the lysozyme-water system," *Biochem.* **18**(12), 2654–2661 (1979).
21. A. Lervik et al., "Heat transfer in protein-water interfaces," *Phys. Chem. Chem. Phy.: PCCP* **12**(7), 1610–1617 (2010).
22. V. Singh et al., "On the thermal elevation of a 60-electrode epiretinal prosthesis for the blind," *IEEE Trans. Biomed. Cir. Sys.* **2**(4), 289–300 (2008).
23. M. Hammer et al., "Optical properties of ocular fundus tissues—an *in vitro* study using the double-integrating-sphere technique and inverse Monte Carlo simulation," *Phys. Med. Biol.* **40**(6), 963–978 (1995).
24. J. Kandulla et al., "Noninvasive optoacoustic online retinal temperature determination during continuous-wave laser irradiation," *J. Biomed. Opt.* **11**(4), 041111 (2006).
25. R. Birngruber, "Choroidal circulation and heat convection at the fundus of the eye: implications for laser coagulation and the stabilization of retinal temperature," in *Laser Applications in Medicine and Biology*, M. L. Wolbarsht, Ed., Vol. **5**, pp. 277–322, Springer, New York (1991).
26. H. Gross, F. Blechinger, and B. Achtner, "Human eye," in *Handbook of Optical Systems: Vol. 4, Survey of Optical Instruments 4* pp. 3–87, Wiley-VCH, Weinheim, Germany (2008).
27. M. Niemz, *Laser-Tissue Interactions: Fundamentals and Applications*, 2nd ed., Springer-Verlag, Berlin (2002).

28. R. L. Vincelette et al., "Thermal lensing in ocular media exposed to continuous-wave near-infrared radiation: the 1150–1350-nm region," *J. Biomed. Opt.* **13**(5), 054005 (2008).

29. R. L. Vincelette et al., "First-order model of thermal lensing in a virtual eye," *J. Opt. Soc. Amer. A* **26**(3), 548–558 (2009).

30. J. Gordon et al., "Long-transient effects in lasers with inserted liquid samples," *J. Appl. Phys.* **36**(1), 3–8 (1965).

31. A. J. Welch and G. D. Polhamus, "Measurement and prediction of thermal injury in the retina of the rhesus monkey," *IEEE Trans. Biomed. Eng.* **BME-31**(10), 633–643 (1984).

32. M. A. Mainster and E. Reichel, "Transpupillary thermotherapy for age-related macular degeneration: long-pulse photocoagulation, apoptosis, and heat shock proteins," *Ophthal. Surg. Las.* **31**(5), 359–373 (2000).

33. A. Narasimhan, K. K. Jha, and L. Gopal, "Transient simulations of heat transfer in human eye undergoing laser surgery," *Intl. J. Heat Mass Trans.* **53**(1–3), 482–490 (2010).

34. J. A. Scott, "A finite element model of heat transport in the human eye," *Phys. Med. Biol.* **33**(2), 227–241 (1988).

35. R. Brinkmann et al., "Real-time temperature determination during retinal photocoagulation on patients," *J. Biomed. Opt.* **17**(6), 061219 (2012).

36. W. Liu et al., "Femtosecond laser pulse filamentation versus optical breakdown in H_2O," *Appl. Phys. B: Las. Opt.* **76**(3), 215–229 (2003).

37. J. Sandeau et al., "Numerical modelling of conductive and convective heat transfers in retinal laser applications.," *J. Biophoton.* **1**(1), 43–52 (2008).

38. J. Sandeau, "Modeling of conductive and convective heat transfers in retinal laser treatments," *Proc. SPIE* **6138**, 61381A (2006).

39. N. Charkoudian, "Skin blood flow in adult human thermoregulation: how it works, when it does not, and why," *Mayo Clinic Proc. Mayo Clinic* **78**(5), 603–612 (2003).

40. A. Jain et al., "Effect of pulse duration on size and character of the lesion in retinal photocoagulation.," *Arch. Ophthal.* **126**(1), 78–85 (2008).

41. D. Lavinsky et al., "Restoration of retinal morphology and residual scarring after photocoagulation," *Acta Ophthalmologica* (in print).

42. M. A. Mainster and E. Reichel, "Transpupillary thermotherapy for age-related macular degeneration: principles and techniques," *Seminars in Ophthal.* **16**(2), 55–59 (2001).

43. D. H. Sliney et al., "What is the meaning of threshold in laser injury experiments? Implications for human exposure limits," *Health Phys.* **82**(3), 335–347 (2002).